



## Optical constants of magnetron sputtered Pt thin films with improved accuracy in the N- and O-electronic shell absorption regions

Soufli, Regina; Delmotte, Franck; Meyer-Ilse, Julia; Salmassi, Farhad; Brejnholt, Nicolai; Massahi, Sonny; Girou, David; Christensen, Finn; Gullikson, Eric M.

*Published in:*  
Journal of Applied Physics

*Link to article, DOI:*  
[10.1063/1.5067366](https://doi.org/10.1063/1.5067366)

*Publication date:*  
2019

*Document Version*  
Publisher's PDF, also known as Version of record

[Link back to DTU Orbit](#)

*Citation (APA):*  
Soufli, R., Delmotte, F., Meyer-Ilse, J., Salmassi, F., Brejnholt, N., Massahi, S., Girou, D., Christensen, F., & Gullikson, E. M. (2019). Optical constants of magnetron sputtered Pt thin films with improved accuracy in the N- and O-electronic shell absorption regions. *Journal of Applied Physics*, 125(8), [085106]. <https://doi.org/10.1063/1.5067366>

---

### General rights

Copyright and moral rights for the publications made accessible in the public portal are retained by the authors and/or other copyright owners and it is a condition of accessing publications that users recognise and abide by the legal requirements associated with these rights.




- Users may download and print one copy of any publication from the public portal for the purpose of private study or research.
- You may not further distribute the material or use it for any profit-making activity or commercial gain
- You may freely distribute the URL identifying the publication in the public portal

If you believe that this document breaches copyright please contact us providing details, and we will remove access to the work immediately and investigate your claim.

# Optical constants of magnetron sputtered Pt thin films with improved accuracy in the N- and O-electronic shell absorption regions

Cite as: J. Appl. Phys. **125**, 085106 (2019); <https://doi.org/10.1063/1.5067366>

Submitted: 17 October 2018 . Accepted: 04 February 2019 . Published Online: 27 February 2019

Regina Soufli , Franck Delmotte , Julia Meyer-Ilse, Farhad Salmassi, Nicolai Brejnholt , Sonny Massahi , David Girou, Finn Christensen, and Eric M. Gullikson



View Online



Export Citation



CrossMark

## ARTICLES YOU MAY BE INTERESTED IN

[Quantum well action model for the formation of a single Shockley stacking fault in a 4H-SiC crystal under non-equilibrium conditions](#)

Journal of Applied Physics **125**, 085705 (2019); <https://doi.org/10.1063/1.5074150>

[Quantitative scanning spreading resistance microscopy on n-type dopant diffusion profiles in germanium and the origin of dopant deactivation](#)

Journal of Applied Physics **125**, 085105 (2019); <https://doi.org/10.1063/1.5066617>

[Enhanced room temperature magneto-caloric effect in Ni-Mn-In films with Fe/Co substitution](#)

Journal of Applied Physics **125**, 085302 (2019); <https://doi.org/10.1063/1.5061704>

Applied Physics Reviews  
Now accepting original research

2017 Journal  
Impact Factor:  
**12.894**



# Optical constants of magnetron sputtered Pt thin films with improved accuracy in the N- and O-electronic shell absorption regions

Cite as: J. Appl. Phys. 125, 085106 (2019); doi: 10.1063/1.5067366

Submitted: 17 October 2018 · Accepted: 4 February 2019 ·

Published Online: 27 February 2019



Regina Soufli,<sup>1</sup> Franck Delmotte,<sup>2</sup> Julia Meyer-Ilse,<sup>3</sup> Farhad Salmassi,<sup>3</sup> Nicolai Brejnholt,<sup>1</sup> Sonny Massahi,<sup>4</sup> David Girou,<sup>4</sup> Finn Christensen,<sup>4</sup> and Eric M. Gullikson<sup>3</sup>

## AFFILIATIONS

<sup>1</sup>Lawrence Livermore National Laboratory, 7000 East Avenue, Livermore, California 94550, USA

<sup>2</sup>Laboratoire Charles Fabry, Institut d'Optique Graduate School, CNRS, Université Paris-Saclay, 91127 Palaiseau Cedex, France

<sup>3</sup>Center for X-Ray Optics, Lawrence Berkeley National Laboratory, 1 Cyclotron Road, Berkeley, California 94720, USA

<sup>4</sup>Danish Technical University (DTU)-Space, Elektrovej 327, DK-2800 Kongens Lyngby, Denmark

## ABSTRACT

We present an experimental, self-consistent determination of the optical constants (refractive index) of Pt using a combination of photoabsorption and reflectance data in the photon energy range 25–778 eV, which includes the N- and O-shell electronic absorption edges of Pt. We compare our new experimental values with Pt optical constant data sets from the literature. Our Pt optical constant values reveal highly resolved absorption-edge fine structure around the O<sub>2,3</sub> and N<sub>6,7</sub> edges in both the absorptive and dispersive portions of the refractive index, which were missing in the earlier literature.

Published under license by AIP Publishing. <https://doi.org/10.1063/1.5067366>

## I. INTRODUCTION

Pt thin films are widely used in optics operating in the extreme ultraviolet (EUV)/soft x-ray range, for example, as single-layer or bi-layer reflective coatings, as transmissive filters, or as the “absorber layer” in multilayer interference coatings, including magnetic multilayers.<sup>1</sup> Pt coatings exhibit high reflectance at grazing and normal incidence angles at EUV/soft x-ray photon energies<sup>2</sup> and have therefore been applied in synchrotron mirrors<sup>3,4</sup> and considered as mirror coatings for space-borne solar physics and astronomy telescopes.<sup>5–9</sup> The photon energies of the above applications include the Pt N- and O-electronic shell absorption edge regions, which extend from 50 eV to 800 eV. Accurate knowledge of the refractive index of Pt in this photon energy region is not only essential for the design and modeling of EUV/x-ray optics containing Pt, but for atomic physics and materials science research in general, especially considering the importance of Pt in catalysis and nanotechnology. At EUV/x-ray energies, the refractive index of materials is defined as

$$n = 1 - \delta + i\beta, \quad (1)$$

where  $1 - \delta$  and  $\beta$  represent the dispersive and absorptive portions of the photon energy-dependent refractive index, respectively. The terms  $\delta$  and  $\beta$  are known as the optical constants.<sup>10</sup> One of the most comprehensive and frequently accessed sources of EUV/x-ray optical constants by the scientific community is Ref. 11, which covers the photon energy range 30 eV–30 keV and is maintained and updated online<sup>12</sup> by the Center for X-ray Optics (CXRO) at Lawrence Berkeley National Laboratory (LBNL). In the CXRO database, measurements of Pt absorption dating from the 1900s to the 1980s have been compiled and interpolated with theoretical calculations; the dispersive part of the Pt refractive index is then calculated via the Kramers-Krönig relation. In the online version of the database,<sup>12</sup> the optical constants of about 15 elements have been updated with recent and more accurately measured photoabsorption values in the vicinity of absorption edges; however, Pt is not among them. More specifically, in the photon energy region of the Pt N- and O-electronic shell absorption edges, the Pt photoabsorption data compilation (and calculated dispersion values) in the CXRO database lacks fine structure details. Another compilation of Pt refractive index data based on reflectance and transmission measurements in the 0.1 eV–2 keV

region, edited by Palik,<sup>13</sup> also lacks fine structure in the Pt N- and O-edge regions. Both Refs. 11 and 13 use a combination of data obtained on bulk Pt and thin Pt films from various works. In the following, we note a few works where the Pt refractive index was determined experimentally in the photon energy regions of Pt N- and O-shell absorption: Haensel *et al.*<sup>14</sup> obtained photoabsorption data on Pt thin films prepared by evaporation. Wehenkel and Gauthé<sup>15</sup> also measured the absorption of Pt thin films via electron energy loss spectra. Birken *et al.*<sup>16</sup> and Windt *et al.*<sup>17</sup> determined experimentally both the absorptive and dispersive parts of the refractive index from reflectance data on Pt thin films prepared by evaporation. The Pt absorption values from Refs. 14 and 17 have been included in the CXRO database. More recently, Pt optical constants based on reflection electron energy-loss spectroscopy (REELS) data were published by Werner *et al.*<sup>18</sup>

This paper presents a new set of Pt optical constants deduced from reflectance and transmittance measurements in the 25–778 eV photon energy range, which includes the Pt N- and O-shell absorption edges. The new Pt optical constants are compared with existing databases and earlier experimental works, referenced in the previous paragraph. Highly resolved absorption-edge fine structure is revealed for the first time in the new Pt measurements.

The new experimental Pt values are combined with earlier data at photon energies below 25 eV and above 778 eV to construct a Pt optical constant data set in the full spectral range. The accuracy of the new data set is examined with electron sum rule tests.

## II. EXPERIMENTAL SETUP

### A. Measurement instrumentation

Grazing Incidence X-Ray Reflectance (GIXR) measurements (discussed in Sec. II B) were performed at Laboratoire Charles Fabry (LCF) with a commercial diffractometer (Bruker<sup>®</sup> Discover D8) equipped with a Cu K $\alpha$  radiation source (photon energy  $E = 8048$  eV), a collimating Göbel mirror, a rotary absorber, Söller and divergence slits, and a scintillator. The reflectance curve is obtained by scanning the grazing incidence angle while tracking the reflected beam ( $\theta$ - $2\theta$  scan configuration). The mechanical angular accuracy and angular resolution are better than 0.01°. The GIXR data are fitted with a genetic algorithm by using the program Leptos<sup>®</sup> in order to deduce several sample parameters: layer thickness, material density, and average interfacial roughness.

The GIXR apparatus at DTU-Space was also used in the measurements discussed in Sec. II B. It is a custom-built device operating at the same photon energy and geometry as mentioned above. The Cu K $\alpha$  x-ray source was manufactured by Rigaku Corporation<sup>®</sup>. The thin film stress measurement apparatus at DTU-Space, used in the measurements discussed in Sec. II B, was a Dektak 150 Stylus Profilometer by Brüker<sup>®</sup>. The apparatus measures changes in the substrate curvature before and after thin film coating and applies Stoney's equation<sup>19</sup> to determine the thin film stress.

The EUV/soft x-ray reflectance and transmittance measurements discussed in Secs. II B, III A, and III B were performed at beamline 6.3.2. of the Advanced Light Source (ALS) synchrotron at LBNL. Beamline 6.3.2. has a grating monochromator with a fixed exit slit and its general characteristics have been described in detail earlier.<sup>20,21</sup> A set of filters of various materials (with each filter selected specifically for each photon energy range) is used for wavelength calibration and 2nd harmonic and stray light suppression. For higher-order harmonic suppression, an “order suppressor” consisting of three mirrors at a variable grazing incidence angle (depending on energy range) and based on the principle of total external reflection is used in addition to the filters. The measurement chamber allows translation of the sample in three dimensions, tilt in two dimensions, and azimuth rotation of the sample holder. The available detectors include various photodiodes and a CCD camera (the latter for sample alignment), which can be rotated by 360° around the axis of the chamber. During the measurements discussed in this paper, a signal was collected with a GaAsP photodiode detector with 1° angular acceptance. The ALS storage ring current was used to normalize the signal against the storage ring current decay. The base pressure in the measurement chamber was 10<sup>-7</sup> Torr. More detailed information on measurements at specific photon energy regions is given below.

The reflectance measurements in the photon energy range 83–188 eV for Pt thickness determination, discussed in Sec. II B, were obtained with the 200 lines/mm grating, a Be filter (83–111 eV), and a B filter (108–188 eV) for 2nd-harmonic and stray light suppression. The order suppressor consisted of 3 C mirrors at 14° (83–111 eV) and 8° (108–188 eV) grazing incidence angle. Photon energy was calibrated based on the L<sub>2,3</sub> absorption edge of a Si filter. The photon beam was 86% s-polarized.

The reflectance measurements for Pt optical constant determination in the photon energy range 25–95 eV, discussed in Sec. III B, were obtained with the 80 lines/mm grating (25–68 eV) and the 200 lines/mm grating (62–95 eV). A Mg filter (25–38 eV), Al filter (42–68 eV), Si filter (62–85 eV), and Be filter (91.84–95 eV) were used for 2nd-harmonic and stray light suppression. The order suppressor consisted of 3 C mirrors at 20° (25–38 eV), 18° (42–68 eV), and 14° (62–95 eV) grazing incidence angle. Photon energy was calibrated based on the L<sub>2,3</sub> absorption edges of an Al and a Si filter. The beam polarization ranged from 93% s-polarized at 25 eV to 89% s-polarized at 95 eV.

For the transmittance measurements discussed in Sec. III A, three gratings (80, 200, and 1200 lines/mm) were used in the monochromator to access the photon energy range 32–778 eV. At photon energies above 270 eV, a 2 mm-diameter pinhole was used in front of the reflectometer chamber to block scattered light from the 1200 lines/mm monochromator grating.

Photon energy calibration was based on the absorption edges of a series of filters (Al, Si, B, Ti, Cr) with a relative accuracy of 0.011% rms and could be determined with 0.007% repeatability. For 2nd harmonic and stray light suppression, a

series of transmission filters (Mg, Al, Si, Be, B, C, Ti, Cr, Co) was used. The order suppressor consisted of three C or Ni mirrors at a grazing incidence angle ranging from  $20^\circ$  to  $6^\circ$ , depending on the photon energy range.

## B. Sample preparation and characterization

The Pt films used in the transmittance measurements were deposited at DTU-Space via DC-magnetron sputtering, using the deposition system described in Ref. 22. All depositions were done with a Pt cathode operated at 600 W with input Ar gas pressure of 2.9 mTorr and rate set to 88 sccm and a base pressure below  $10^{-6}$  Torr. Each Pt film was deposited on a photoresist-coated, 100-mm diameter Si wafer substrate with (100) orientation and 525–550  $\mu\text{m}$  thickness. After Pt deposition, the samples that were transported at CXRO/LBNL, where stainless steel support rings 8 mm in diameter with a 3 mm diameter opening, were glued onto the coated wafers using acetone-resistant glue. The samples were then soaked in acetone for a few minutes. This process results in producing free-standing Pt films mounted on the support rings, with a 3-mm-diameter area available for transmittance measurements. This method has also been implemented in the earlier work<sup>23–26</sup> to produce free-standing thin films for EUV/x-ray optical constant studies.

For atomic composition and thin film stress characterization purposes, two witness samples (for each transmittance sample) were also coated with Pt at DTU-Space. The witness substrates were Si wafer pieces, and during deposition, they were located next to the photoresist-coated Si wafer substrate used for the transmittance sample. Thin film stress measurements performed at DTU-Space determined that the stress of all Pt films discussed in this paper was in the  $-700$  to  $-800$  MPa range (compressive). The atomic composition of the Pt films deposited at DTU was determined via Rutherford Backscattering (RBS) measurements with 2.275 MeV  $\text{He}^{++}$  ions and a backscattering angle of  $160^\circ$ , performed at EAG Labs (Sunnyvale, California), on a Pt witness sample of 48.4 nm thickness (determined experimentally at DTU-Space by fitting GIXR data). The atomic composition of the sample was thus found to be 99% Pt, 0.6% Fe, and 0.4% Ar, with Fe and Ar believed to have been incorporated in the film during deposition. The density of the Pt films deposited at DTU-Space was determined via fitting of GIXR data (obtained at DTU-Space and at LCF) on Pt transmittance and witness samples and was found to be  $21.45 \pm 0.20$  g/cm<sup>3</sup>, which corresponds to the Pt bulk density. Four Pt samples (T1, T2, T6, and T7) were used in the transmittance measurements. The sample thicknesses and their surface and interface micro-roughness were verified experimentally (i) by GIXR measurements at DTU-Space, while the Pt thin films were on the photoresist-coated Si substrate (ii) by reflectance vs. photon energy measurements in the photon energy range 83–188 eV carried out at beamline 6.3.2. of the ALS at LBNL. It should be noted that these ALS reflectance measurements were aiming to determine only the Pt thickness and roughness, not the Pt optical constants (reflectance measurements for Pt optical constants are

discussed in Sec. III B). The ALS reflectance measurements were performed at two different angles ( $65^\circ$  and  $85^\circ$  from grazing) on Pt free-standing films, i.e., after removal from the photoresist coated Si substrate. Due to limitations in the geometry of the sample holder, the ALS reflectance measurements were performed with the photon beam incident on the Pt surface side, which was earlier (before removal from the substrate) in contact with the photoresist. The ALS reflectance data and corresponding models on two of the samples (T2 and T7) are shown in Fig. 1. All GIXR and ALS reflectance measurements were modeled using the IMD software package<sup>27</sup> and the results are summarized in Table I. For samples T1 and T6, the agreement between modeled Pt film thicknesses from GIXR and ALS data is excellent. In samples T2 and T7, the absence of well-defined interference fringes (due to the much larger Pt thickness) prevented modeling of the Pt thickness via GIXR measurements. In the ALS data, a residual photoresist layer (i.e., photoresist that has remained on the Pt surface after removal from the substrate) was

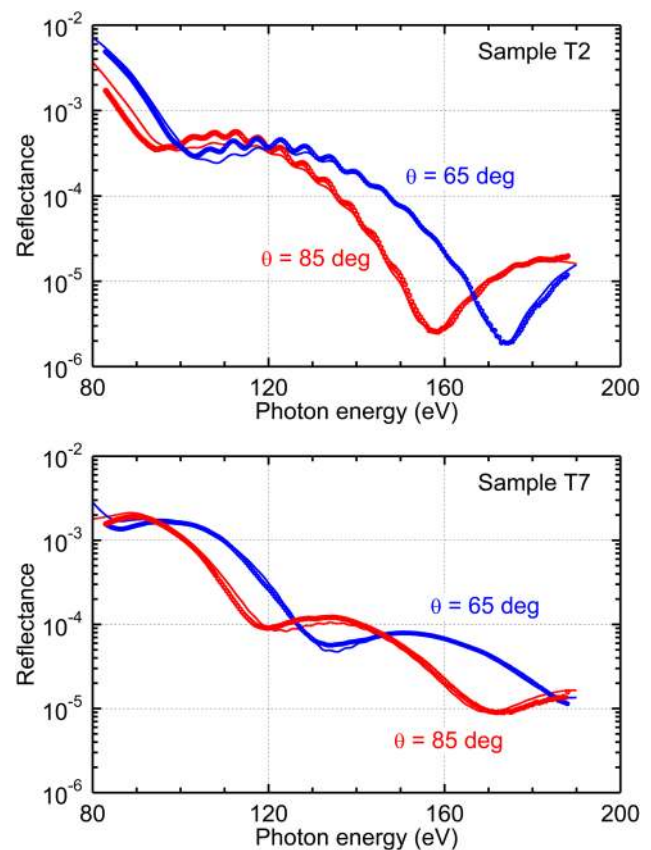


FIG. 1. Reflectance data obtained at ALS beamline 6.3.2. (points) and IMD models<sup>27</sup> (solid lines) are plotted in a lin-log scale for two of the Pt thin film samples. The model parameters are summarized in Table I. Optical constant values for the models were obtained from the CXRO database.<sup>12</sup>



**TABLE I.** Thin film parameters deduced from GIXR and reflectance data.  $\rho_1$ ,  $z_1$ , and  $\sigma_1$  are the residual photoresist density, thickness, and roughness at the vacuum/photoresist interface.  $z_2$ ,  $\sigma_2$ , and  $\sigma_3$  are the Pt thickness and roughness at the photoresist/Pt and Pt/vacuum interfaces. A Pt density of  $21.45 \text{ g/cm}^3$  was used in the models, determined by GIXR measurements.

	Residual photoresist			Pt		
	$\rho_1$ ( $\text{g/cm}^3$ )	$z_1$ (nm)	$\sigma_1$ (nm rms)	$z_2$ (nm)	$\sigma_2$ (nm rms)	$\sigma_3$ (nm rms)
T7 65°	1.436	13.37	0.94	202.55 <sup>a</sup>	0.63	1.33
T7 85°	1.4	13.41	0.94	202.55 <sup>a</sup>	0.63	1.33
<b>T7 average</b>	<b>1.418</b>	<b>13.39</b>	<b>0.94</b>	<b>202.55<sup>a</sup></b>	<b>0.63</b>	<b>1.33</b>
T6 65°	1.42	12.91	1.04	53.05	0.95	1.33
T6 85°	1.42	13.03	1.08	52.58	0.88	1.35
<b>T6 average</b>	<b>1.42</b>	<b>12.97</b>	<b>1.06</b>	<b>52.815</b>	<b>0.915</b>	<b>1.34</b>
<b>T6 GIXR</b>				<b>52.46</b>		
T2 65°	1.42	10.49	0.64	103.44	0.76	1.49
T2 85°	1.42	10.4	0.72	103.49	0.73	1.61
<b>T2 average</b>	<b>1.42</b>	<b>10.45</b>	<b>0.68</b>	<b>103.47</b>	<b>0.75</b>	<b>1.55</b>
T1 65°	1.42	10.63	0.78	54.11	0.71	1.47
T1 85°	1.42	10.59	0.92	54.15	0.74	1.6
<b>T1 average</b>	<b>1.42</b>	<b>10.61</b>	<b>0.85</b>	<b>54.13</b>	<b>0.73</b>	<b>1.54</b>
<b>T1 GIXR</b>				<b>54.33</b>		

<sup>a</sup>The thickness of sample T7 was determined from transmittance measurements, as discussed in Sec. III A.

derived on the surface of all samples. This photoresist layer was modeled as having a density of  $1.42 \text{ g/cm}^3$ , consistent among all ALS reflectance measurements and an average thickness of  $11.85 \text{ nm}$ , determined among samples T1, T2, T6, and T7 (see Table I). The atomic composition of the residual photoresist layer was determined from the transmittance measurements discussed later in Sec. III A and was entered in the ALS reflectance data models. In sample T7, the Pt layer was too thick for interference fringes to be visible in the ALS reflectance or GIXR data. The ALS reflectance data on sample T7 were thus used only to model the residual photoresist layer density and thickness. The Pt thickness of sample T7 was determined using transmittance data (see Sec. III A). We estimate that the accuracy in the thickness determination of the Pt and residual photoresist layers is about  $\pm 1\%$ .

The Pt sample used in the reflectance vs. incidence angle measurements in the 25–95 eV range at ALS beamline 6.3.2. for optical constants determination, discussed in Sec. III B, was deposited at CXRO in a DC-magnetron sputtering system with planar geometry, on a fused silica substrate with 25 mm diameter and 6 mm thickness. The density of the CXRO Pt coating was verified by GIXR measurements at LCF and was found to be  $21.45 \pm 0.20 \text{ g/cm}^3$ , the same as the Pt samples deposited at DTU-Space. The thickness of the coating was determined by fitting ALS reflectance and GIXR data and is discussed in detail in Sec. III B.

All GIXR and ALS reflectance data discussed in this work were modeled/fitted with the Fresnel equations for the reflected field intensities. Surface and interface roughness were assumed to have an error function profile in the models, as discussed in detail in Ref. 27. All fits to GIXR and ALS

reflectance and transmittance data used material optical constant values from the CXRO database.<sup>12</sup>

### III. PT OPTICAL CONSTANTS: RESULTS AND DISCUSSION

#### A. Pt optical constants from transmittance measurements

Figure 2 shows the transmittance measurement results on free-standing samples T6, T1, T2, and T7 with Pt thicknesses of 52.46, 54.13, 103.47, and 202.55 nm, respectively. The methodology used in this paper has also been implemented and described in detail in the earlier work.<sup>23–26</sup> The transmittance curves in Fig. 2 were obtained through the expression  $T = I/I_0$  for the transmittance  $T$  of a film at a given photon energy, where  $I$  is the intensity transmitted through the film and  $I_0$  is the intensity of the incident photon beam. Transmittance measurements were obtained in steps ranging from 0.1 to 0.5 eV, depending on the photon energy range. The position of the photon beam was monitored so that data would be collected from the same area on each sample at all photon energy ranges, resulting in measurement reproducibility better than 0.5%. Samples T1 and T6 have similar thicknesses; nevertheless, they were both measured (as is shown in Fig. 2) to demonstrate the reproducibility and consistency of our measurement methodology. The energy-dependent, absorptive portion  $\beta$  of the refractive index of the sputtered Pt thin film was obtained through the expression

$$T = T_0 \exp(-4\pi\beta x/\lambda), \quad (2)$$

where  $x$  is the thickness of the Pt layer,  $\lambda$  is the photon wavelength (related to the photon energy  $E$  by  $E = hc/\lambda$ ), and  $T_0$  is the transmittance from layers other than Pt, which may be present on the sample.

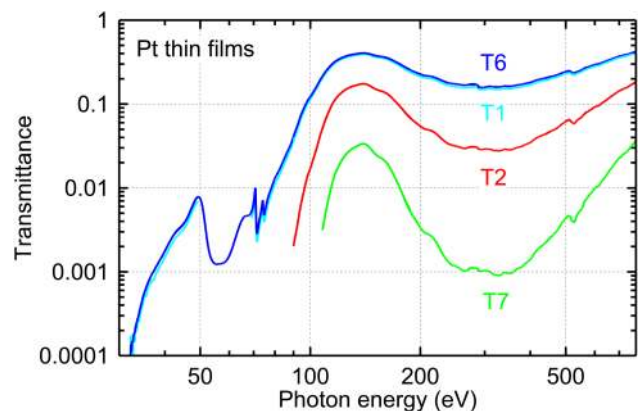


**FIG. 2.** Experimental transmittance results obtained at ALS beamline 6.3.2. on 4 free-standing Pt thin films are plotted in a log-log scale.

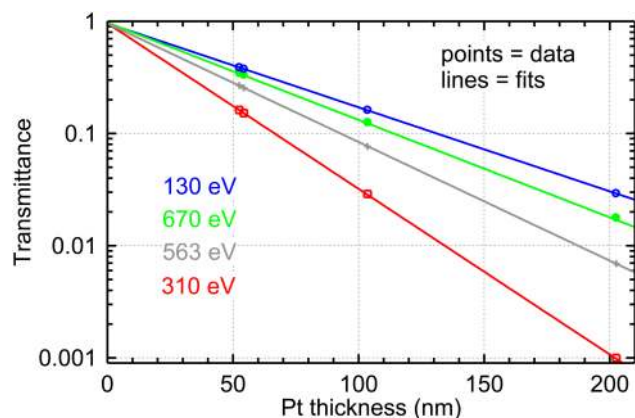


**FIG. 3.** Fitted curves (lines) to experimental transmittance data points from Pt thin films are shown at 4 different photon energies, in a lin-log scale. Transmittance data are displayed as follows: 130 eV (blue circles), 670 eV (green filled circles), 563 eV (grey plus signs), and 310 eV (red squares).

An example of the fitting procedure to determine  $\beta$  using Eq. (2) is shown in Fig. 3, for four different photon energies. In the plot of the measured transmittance  $T$  (on a logarithmic scale) vs. Pt thickness  $x$  at a given photon energy, the data points are fitted to a straight line whose slope is equal to  $4\pi\beta/\lambda$ . Furthermore, the point where the straight line intercepts the  $y$ -axis corresponds to the transmittance  $T_0$  at Pt thickness  $x = 0$ , assuming that the thickness of the overlayer responsible for  $T_0$  is nearly the same for all samples used in the measurements. The Pt thickness of samples T1, T2, and T6 was determined via the ALS reflectance and GIXR measurements discussed in Sec. II B and shown in Table I. The Pt thickness of sample T7 was adjusted around a nominal thickness of 200 nm, in order to maximize the regression factor of the transmittance-vs-thickness fits to the experimental data points, in the energy range 560 eV–770 eV (which is free of absorption edges). This method determined a Pt thickness of 202.55 nm for sample T7 and this thickness value resulted in a regression factor very close to 1 in the fits at all photon energies where transmittance data were obtained. The above-mentioned procedure to determine  $\beta$  for Pt using transmittance data from samples T1, T2, T6, and T7 was applied in the photon energy range 108–778 eV. At photon energies below 108 eV, data from samples T1 and T6 only were used, as the much thicker samples T2 and T7 produced transmitted signal values that were very “noisy” and thus unsuitable for use with the above method. For this reason, in the photon energy range 32–108 eV,  $\beta$  was determined via Eq. (2) from transmittance data on sample T6 only, using the layer parameters in Table I for the Pt layer and residual photoresist layer—the transmittance of the latter represents  $T_0$  in Eq. (2). Similar results were obtained when  $\beta$  was determined from transmittance data on sample T1 only, in the range 32–108 eV.

As discussed in Sec. II A, the quantity  $T_0$  in Eq. (2) was determined to be the result of a residual photoresist layer on

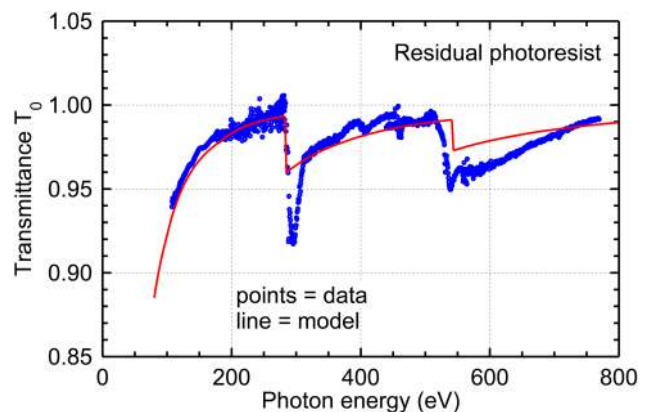


**FIG. 4.** Experimental results (points) are shown for the transmittance  $T_0$  contributed by overlayers of residual photoresist on samples T1, T2, T6, and T7. The solid line is a model to the experimental results, for a layer of composition C:H:O = 1:1:1, density  $\rho = 1.42 \text{ g/cm}^3$ , and thickness  $z = 11.85 \text{ nm}$ . Optical constant values for the model were obtained from the CXRO database.<sup>12</sup>

each Pt sample. A plot of the results for  $T_0$  vs. photon energy derived from the transmittance data on samples T1, T2, T6, and T7 discussed earlier in this section is shown in Fig. 4. It includes a curve calculated to model the experimental results for  $T_0$ , corresponding to a 11.85 nm-thick overlayer consisting of C:H:O = 1:1:1 with a density of  $1.42 \text{ g/cm}^3$ . These values are consistent with the overlayer parameters determined by fitting ALS reflectance and GIXR data on samples T1, T2, T6, and T7, discussed in Sec. II A and shown in Table I. The model constructed for  $T_0$  in Fig. 4 was employed to calculate  $T_0$  in the photon energy range 32–108 eV, where  $\beta$  was determined from sample T6 only, via Eq. (2).

Figure 5 shows a plot of  $\beta$  vs. photon energy obtained by transmittance measurements in this work, compared with those from the CXRO database<sup>12</sup> and from Haensel *et al.*,<sup>14</sup> the latter being the only earlier measurements we could find where the photoabsorption of Pt exhibits the splitting at the Pt  $N_{6,7}$  absorption edge. Interestingly, although the data by Haensel *et al.* were part of the compilation included in the CXRO database, the Pt  $N_{6,7}$  edge splitting is absent in the CXRO database, presumably due to the smoothing incurred by the combination of various data sets and the interpolation of data points with theoretical calculations. Figure 5 reveals significant differences between the present experimental Pt photoabsorption data and the CXRO values, especially at photon energies below 200 eV. The values from Haensel *et al.* are consistently higher (up to a factor of 2) than the present data, at photon energies above 70 eV.

## B. Pt optical constants from reflectance measurements

Reflectance measurements were performed in the range 25–95 eV on the CXRO Pt sample discussed in Sec. II B, in

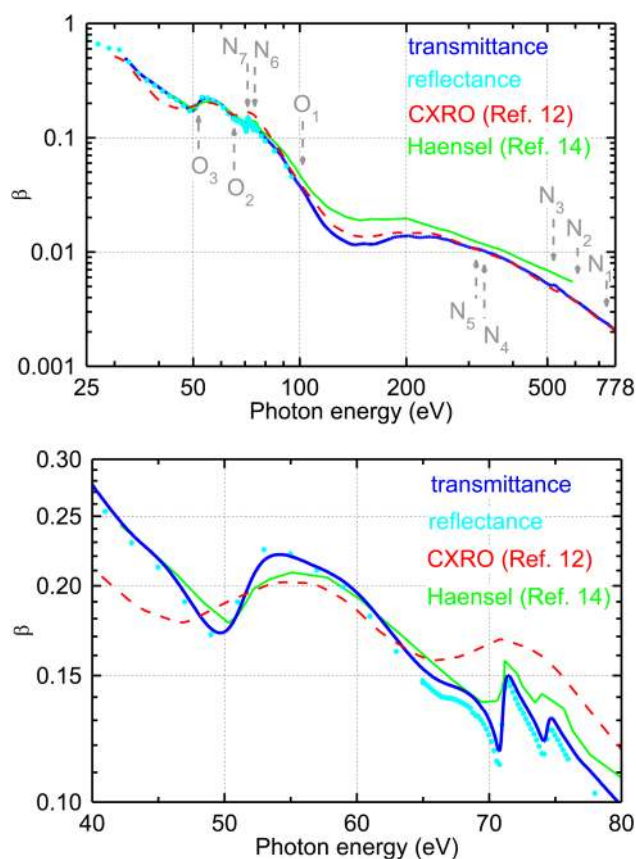


**FIG. 5. Top:** The absorption  $\beta$  of sputtered Pt thin films determined in this work by transmittance (blue solid line) and reflectance (cyan circles) is plotted vs. photon energy in a log-log scale. Tabulated values from the CXRO database<sup>22</sup> (red dashed line) and earlier experimental data from Haensel *et al.*<sup>14</sup> (green solid line) are also shown for comparison. The arrows indicate the photon energies of the Pt N- and O-shell absorption edges. **Bottom:** A detail of the top plot is shown in a lin-log scale, in the vicinity of the Pt O<sub>2,3</sub> and N<sub>6,7</sub> absorption edges.

order to determine the Pt optical constants with a method that is independent to the transmittance measurements discussed in Sec. III A. It should be noted that the reflectance method determines both  $\delta$  and  $\beta$  experimentally, while the transmittance method determines only  $\beta$  experimentally and relies on additional absorption data sets from other works (at lower and higher energies) and on the Kramers-Krönig transformation, for  $\delta$ . The photon energy range for the reflectance measurements was chosen to overlap with and extend the low-energy side of the transmittance measurements of Sec. III A, especially since in this work there was a lack of Pt samples that would be thin enough to produce useful transmittance data at low energies. Reflectance vs. incidence angle scans were performed at 85 different photon energies, in 2 eV or 0.2 eV increments, the latter in the region of the O<sub>2</sub> and N<sub>6,7</sub> absorption edges. In each reflectance scan, the incidence angle range was 1–88° in 1° steps. The experimental

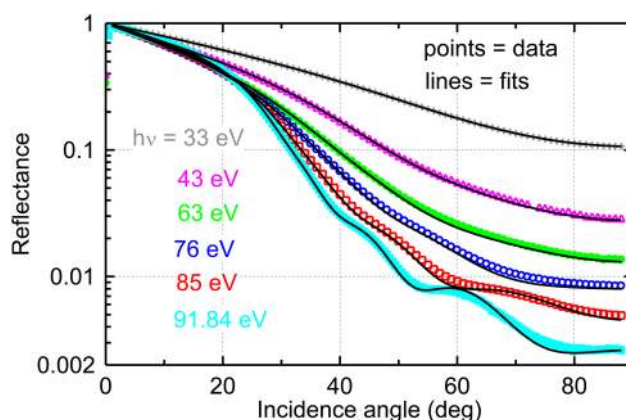


**FIG. 6.** Measured reflectance vs. incidence angle data are plotted in a lin-log scale at 6 different photon energies, for a 31.37-nm-thick Pt thin film deposited on a fused silica substrate. Reflectance data are displayed as follows: 33 eV (grey plus signs), 43 eV (magenta triangles), 63 eV (green filled circles), 76 eV (blue circles), 85 eV (red squares), 91.84 eV (cyan filled squares). The fits to the data (solid lines) were used to determine  $\delta$  and  $\beta$  for Pt at each photon energy.

reflectance curves were fitted with the Fresnel equations for the reflected field intensities by means of a least-squares fitting algorithm.<sup>28</sup> First, reflectance vs. angle data at 5 photon energies were fitted for the Pt optical constants  $\delta$ ,  $\beta$  as well as for the thickness of the Pt layer, using the IMD software.<sup>27</sup> Regarding the fused silica substrate of the CXRO Pt sample, the tabulated density (2.19 g/cm<sup>3</sup>) and a surface micro-roughness of 0.2 nm rms (determined via surface metrology) were entered as fixed parameters in all fits. Based on the results of these 5 fits, the average thickness of the Pt layer was determined to be 31.37 nm with a standard deviation of 0.13 nm. The same procedure was applied to determine the micro-roughness of the Pt layer, by fitting reflectance vs. angle data at 9 different photon energies, resulting in a roughness of 0.58 nm with a standard deviation of 0.05 nm. These Pt thickness and roughness values were also confirmed by GIXR measurements at LCF. The Pt thickness and roughness values were then entered as fixed parameters in all 85 reflectance vs. angle scans, which were fitted for the optical constants  $\delta$ ,  $\beta$  of Pt using the Fresnel equations and custom-written software, to facilitate the efficient fitting of 85 scans. Six representative reflectance scans and their fits are shown in Fig. 6. The high quality of the fits is noteworthy, especially at low incidence angles, which largely determine the values of  $\delta$ ,  $\beta$  at each photon energy. The resulting values for  $\beta$  of Pt in the range 25–95 eV are plotted in Fig. 5, together with the values determined by transmittance in Sec. III A. The agreement between  $\beta$  values determined by reflectance and transmittance in this work is very good, which provides confidence in the data obtained by both methodologies. This is especially remarkable, if one takes into account that (i) optical constants (especially  $\beta$ ) obtained by reflectance can be sensitive to surface roughness



and contamination of the measured sample and (ii) the reliability of reflectance data fits may be diminished at photon energy regions, where  $\beta \geq \delta$  (such as the region 25–95 eV of the current Pt reflectance measurements) and especially near absorption edges, where the values of  $\delta$  and  $\beta$  change abruptly.<sup>28,29</sup>

### C. Compilation of a new Pt optical constant data set

Provided a set of photoabsorption values ( $\beta$ ) is available in the full spectral range, i.e., from photon energies  $E \rightarrow 0$  to  $E \rightarrow \infty$ , then  $\delta$  can be calculated by the Kramers-Krönig relation<sup>10,30</sup>

$$\delta(E) = -\frac{2}{\pi} P \int_0^{\infty} \frac{E' \beta(E')}{E'^2 - E^2} dE', \quad (3)$$

where  $P$  denotes the Cauchy principal value of the integral. Based on the results and analysis presented in Secs. III A and III B, a data set of new experimental values for  $\beta$  of Pt was constructed in the photon energy range 25–778 eV, containing the following: (i) in the region 25–31 eV, values determined from the reflectance measurements discussed in Sec. III B, (ii) in the region 32–108 eV, values determined from the transmittance measurements on sample T6 discussed in Sec. III A, and (iii) in the region 108–778 eV, values determined from the transmittance measurements on samples T1, T2, T6, and T7 discussed in Sec. III A. Outside the range 25–778 eV,  $\beta$  values from the earlier literature were employed, as follows: (i) In the region  $10^{-4}$ –0.09 eV, theoretical calculations by Rakic *et al.*<sup>31</sup> based on the Lorenz-Drude model, (ii) in the region 0.1–21.4 eV, data compiled by Palik,<sup>13</sup> (iii) in the region 811 eV–14.3 keV, tabulated values from CXRO,<sup>12</sup> and (iv) in the region 14.4 keV–433 keV, tabulated data from the National Institute of Standards and Technology (NIST).<sup>32</sup> This approach, including the choice of data from the above references, was recently employed successfully to determine the optical constants of Cr.<sup>33</sup> Figure 7 shows a plot of the above-mentioned composite data set for  $\beta$  of Pt, demonstrating good continuity between the different sets of  $\beta$  values. These  $\beta$  values were employed to calculate  $\delta$  via Eq. (3). The resulting  $\delta$  values are plotted vs. photon energy in Fig. 8 (left column) alongside the corresponding  $\beta$  values in the right column and are compared with  $\delta$  and  $\beta$  values from the earlier literature.<sup>12,13,17,18</sup> In Fig. 8 (top left), we note the good agreement between the new  $\delta$  values determined directly via reflectance measurements (Sec. III B) and new  $\delta$  values calculated from transmittance measurements via the Kramers-Krönig relationship [Eq. (3)]. The agreement is noteworthy especially considering that the Kramers-Krönig relationship may include errors contributed from  $\beta$  values in the entire spectrum. The new  $\delta$  values exhibit pronounced differences with earlier data in the vicinity of the O<sub>2,3</sub> and N<sub>6,7</sub> edges—the splitting around the Pt N<sub>6,7</sub> edge is observed for the first time in the literature. In Fig. 8 (top right), we note again the agreement between  $\beta$  values from reflectance and transmittance measurements in this work and the significant differences with the earlier literature.

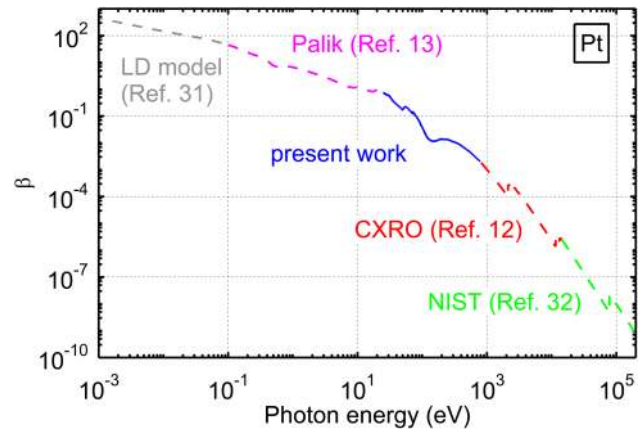


FIG. 7. Shown is a composite data set of theoretical and experimental  $\beta$  values, plotted in a log-log scale and used to calculate  $\delta$  in Eq. (5): (i) Lorenz-Drude (LD) model<sup>31</sup> (grey dash line), (ii) data compilation by Palik *et al.*<sup>13</sup> (magenta dash line), (iii) experimental data from this work (blue solid line), (iv) tabulated values from CXRO<sup>12</sup> (red dash line), and (v) tabulated values from NIST<sup>32</sup> (green dash line).

Similarly, in Fig. 8 (bottom), both  $\delta$  and  $\beta$  exhibit significant differences with earlier data, in the region 95–778 eV. The absence of fine structure around the Pt N<sub>4,5</sub> edge is evident in Fig. 8 (bottom) and in Fig. 5 (top). This has also been observed by Haensel *et al.*,<sup>14</sup> who mention that the increased absorption taking place in that photon energy region (due to electronic transitions occurring at lower photon energies) may be masking the Pt N<sub>4,5</sub> transition. Finally, in Fig. 9, we present a comparison of the data from the present work with the data from Birken *et al.*,<sup>16</sup> where the real and imaginary parts of the Pt dielectric function were determined experimentally via reflectance vs. incidence angle measurements using the same method as discussed in Sec. III B of this paper. The dielectric function  $\epsilon$  of a material is defined as

$$\epsilon = \epsilon_1 + i\epsilon_2 = n^2; \quad (4)$$

therefore, from Eqs. (1) and (4), we obtain  $\epsilon_1 = (1 - \delta)^2 - \beta^2$  and  $\epsilon_2 = 2(1 - \delta)\beta$ .

Figure 9 demonstrates remarkable agreement between the results of this work and Ref. 16, for both real and imaginary parts of the Pt dielectric function, thus providing an additional validation of our measurements. Nevertheless, the photon energy spacing of the data points from Ref. 16 is not adequate to resolve the fine structure around the Pt N- and O-edges, which is present in the data from this paper.

The standard method to test the consistency of the composite set of  $\beta$  values used in the Kramers-Krönig relation [Eq. (3)] is to calculate the effective number of electrons ( $N_{eff}$ ) contributing to the absorption processes in the atom at all

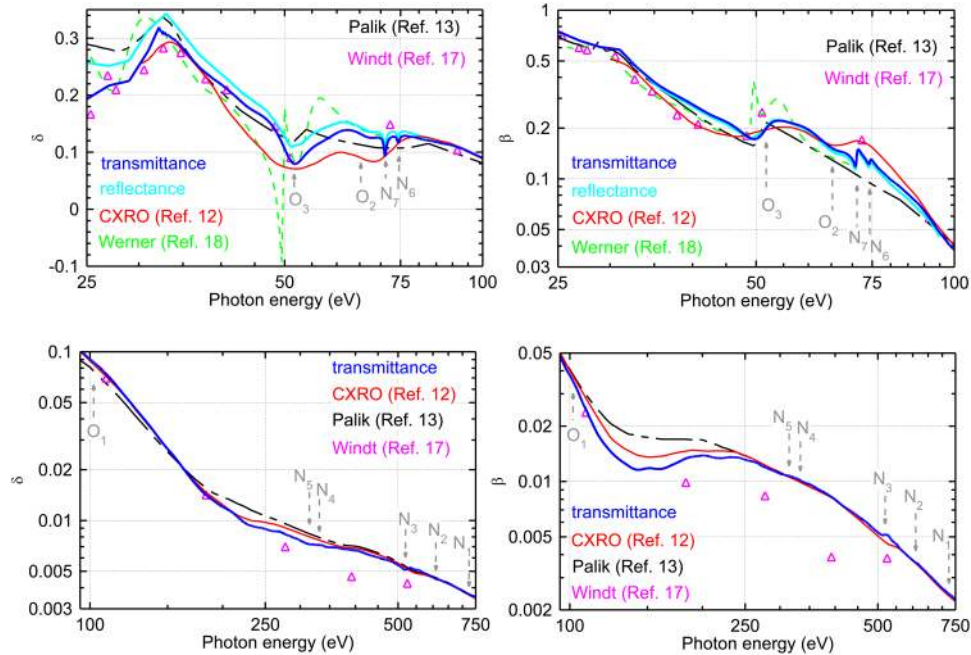


**FIG. 8.** The Pt optical constants  $\delta$  (left) and  $\beta$  (right) derived from transmittance (blue solid line) and reflectance (cyan solid line) measurements in this work are plotted vs. photon energy in the range 25–100 eV (top) and 100–778 eV (bottom). Data from the references are also plotted, for comparison: Ref. 12 (red solid line), Ref. 13 (black dashed-dotted line), Ref. 17 (magenta triangles), and Ref. 18 (green dashed line). The arrows indicate the photon energies of the Pt N- and O-shell absorption edges. The top left plot is in a log-linear scale, while the rest are in a log-log scale.

photon energies from 0 to  $\infty$  via the equation<sup>34</sup>

$$N_{eff} = \frac{4m\epsilon_0}{\pi n_a e^2} \int_0^\infty E' \beta(E') dE', \quad (5)$$

where  $n_a$  is the atomic density of the material,  $m$  and  $e$  are the electron mass and charge, respectively, and  $\epsilon_0$  is the vacuum permittivity. If the  $\beta$  data are accurate in the entire spectral range, then Eq. (5) produces  $N_{eff} = Z^* = Z - (Z/82.5)^{2.37}$ , which is the so-called  $f$ -sum rule, where  $Z^*$  represents the atomic number  $Z$  corrected by the relativistic effect.<sup>11</sup> For Pt atoms,  $Z^* = 77.12$ . Using the composite set of  $\beta$  values plotted in Fig. 7 and discussed above, including our new experimental data in the range 25 eV–778 eV, we obtain  $N_{eff} = 76.09$  from Eq. (5). This result demonstrates a deficiency of only 1.03 electrons (1.3%) from the ideal 77.12 electrons and thus a very good overall consistency of our composite Pt photoabsorption data set. If we replace our experimental data in the range 25 eV–778 eV with the CXRO tabulated values,<sup>12</sup> we obtain  $N_{eff} = 76.19$ . The difference between the two  $N_{eff}$  results is 0.1 electrons, which represents 0.13% of the  $Z^*$  value for Pt. This difference is too small and well within the error bars of both data sets; therefore, it is not meaningful towards assessing the accuracy of one data set vs. the other. For example, 1% uncertainty in the density of the Pt films in the photon

energy region 25–778 eV would produce 0.36 electrons difference in  $N_{eff}$  in Eq. (5). Furthermore, it should be noted that Eq. (5) is useful toward pointing deficiencies in absorption data from the overall spectrum, without any specificity on

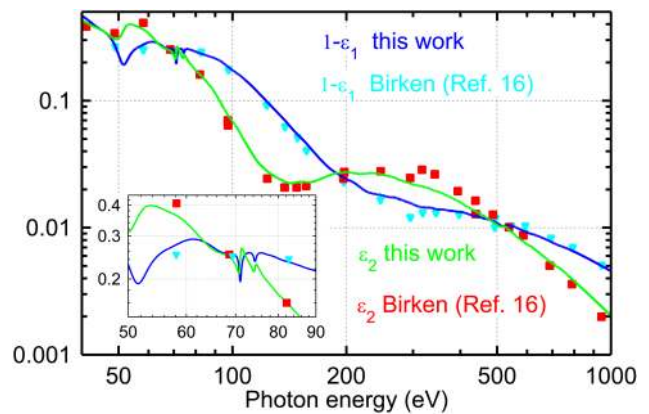


**FIG. 9.** Data for  $(1 - \epsilon_1)$  and  $\epsilon_2$  (of the dielectric function  $\epsilon = \epsilon_1 + i\epsilon_2$ ) of Pt thin films from this work (solid lines) and from Birken *et al.*<sup>16</sup> (data points) are plotted vs. photon energy in a log-log scale. The inset is a detail of the plot in the photon energy region of the Pt  $O_{2,3}$  and  $N_{6,7}$  absorption edges.

localized photon energy regions. As can be seen in Fig. 5, our new experimental  $\beta$  values are higher than the CXRO tabulated values in some photon energy regions and lower in other regions, thus resulting in a near-zero net difference between the two sets, when the sum rule of Eq. (5) is applied. Reference 35 has proposed a method to evaluate optical constant data sets in specific photon energy regions, using “window functions.”

#### IV. CONCLUSIONS

We have measured the optical constants ( $\delta$ ,  $\beta$ ) of Pt via transmittance and reflectance measurements in the region of the Pt N- and O-shell absorption edges. We have combined our photoabsorption data with values from the literature at photon energies outside our measurement range and have employed the Kramers-Krönig transformation to produce a self-consistent set of ( $\delta$ ,  $\beta$ ) values for Pt in the entire spectrum. Our experimental data demonstrate for the first time highly resolved fine structure in the region of the Pt O<sub>2,3</sub> and N<sub>6,7</sub> edges, resulting in differences of up to a factor of 2 compared to earlier published Pt optical constant values. The new ( $\delta$ ,  $\beta$ ) values for Pt determined in this work are available upon request at [regina.soufli@llnl.gov](mailto:regina.soufli@llnl.gov).

#### ACKNOWLEDGMENTS

This work was supported by a NASA project (No. 13-APRA13-0091), by a STSM Grant from COST Action MP1203, by the Jean d'Alembert fellowship program from Université Paris-Saclay, and by Lawrence Livermore National Laboratory (LLNL)'s Professional Research and Teaching leave program. This work was performed under the auspices of the U.S. Department of Energy by Lawrence Livermore National Laboratory under Contract No. DE-AC52-07NA27344 and by the University of California Lawrence Berkeley National Laboratory under Contract No. DE-AC03-76F00098. The authors are thankful to Stefan Immler (NASA) and Marie-Anne Descalle and Stefan Hau-Riege (LLNL) for their support of this project.

#### REFERENCES

<sup>1</sup>N. Nakajima, T. Koide, T. Shidara, H. Miyauchi, H. Fukutani, A. Fujimori, K. Iio, T. Katayama, M. Nyvlt, and Y. Suzuki, “Perpendicular magnetic anisotropy caused by interfacial hybridization via enhanced orbital moment in Co/Pt multilayers: Magnetic circular X-ray dichroism study,” *Phys. Rev. Lett.* **81**, 5229–5232 (1998).  
<sup>2</sup>W. R. Hunter, “Reflectance spectra of single materials,” in *Vacuum Ultraviolet Spectroscopy*, edited by J. A. R. Samson and D. L. Ederer (Academic Press, San Diego, 1998), pp. 212–213.  
<sup>3</sup>V. Rehn and V. O. Jones, “Vacuum ultraviolet (VUV) and soft X-ray mirrors for synchrotron radiation,” *Opt. Eng.* **17**, 175504 (1978).  
<sup>4</sup>T. Koide, S. Sato, T. Shidara, M. Niwano, M. Yanagihara, A. Yamada, A. Fujimori, A. Mikuni, H. Kato, and T. Miyahara, “Investigation of carbon contamination of synchrotron radiation mirrors,” *Nucl. Instrum. Methods Phys. Res. A* **246**, 215–218 (1986).  
<sup>5</sup>T. R. Gull, H. Herzig, J. F. Osantowski, and A. R. Toft, “Low earth orbit environmental effects on osmium and related optical thin-film coatings,” *Appl. Opt.* **24**, 2660–2665 (1985).

<sup>6</sup>H. Herzig, A. R. Toft, and C. M. Fleetwood, “Long-duration orbital effects on optical coating materials,” *Appl. Opt.* **32**, 1798–1804 (1993).  
<sup>7</sup>G. Pareschi, V. Cotroneo, D. Spiga, D. Vernani, M. Barbera, M. Antonella Artale, A. Collura, S. Varisco, G. Grisoni, G. Valsecchi, and B. Negri, “Astronomical soft x-ray mirrors reflectivity enhancement by multilayer coatings with carbon overcoating,” *Proc. SPIE* **5488**, 481–491 (2004).  
<sup>8</sup>T. Sakao, N. Narukage, Y. Suematsu, K. Watanabe, M. Shimojo, S. Imada, S. Ishikawa, and E. E. DeLuca, “The soft x-ray photon-counting telescope for solar observations,” *Proc. SPIE* **9144**, 91443D (2014).  
<sup>9</sup>D. Della Monica Ferreira, A. C. Jakobsen, S. Massahi, F. E. Christensen, B. Shortt, J. Garnæs, A. Torras-Rosell, M. Krumrey, L. Cibik, and S. Marggraf, “X-ray mirror development and testing for the ATHENA mission,” *Proc. SPIE* **9905**, 99055 K (2016).  
<sup>10</sup>D. Attwood and A. Sakdinawat, *X-rays and Extreme Ultraviolet Radiation Principles and Applications* (Cambridge University Press, 2017), pp. 60–108.  
<sup>11</sup>B. Henke, E. Gullikson, and J. Davis, “X-ray interactions: Photoabsorption, scattering, transmission, and reflection at E = 50–30000 eV, Z = 1–92,” *At. Data Nucl. Data Tables* **54**, 181–342 (1993).  
<sup>12</sup>See [http://henke.lbl.gov/optical\\_constants/](http://henke.lbl.gov/optical_constants/) for an updated version of Ref. 11.  
<sup>13</sup>D. W. Lynch and W. R. Hunter, “Comments on the Optical constants of metals and an introduction to the data for several metals,” in *Handbook of Optical Constants of Solids*, edited by E. D. Palik (Academic Press, San Diego, 1998), Vol. 1, pp. 333–341.  
<sup>14</sup>R. Haensel, K. Radler, B. Sonntag, and C. Kunz, “Optical absorption measurements of tantalum, tungsten, rhenium and platinum in the extreme ultraviolet,” *Solid State Commun.* **7**, 1495–1497 (1969).  
<sup>15</sup>C. Wehenkel and B. Gauthé, “Optical absorption coefficient of nickel, palladium platinum and copper, silver, gold between 20 and 120 eV,” *Opt. Commun.* **11**, 62–63 (1974).  
<sup>16</sup>H. G. Birken, C. Blessing, C. Kunz, and R. Wolf, “Investigations on the consistency of optical constants in the XUV determined by different methods,” *Rev. Sci. Instrum.* **60**, 2223–2226 (1989).  
<sup>17</sup>D. L. Windt, W. C. Cash, M. Scott, P. Arendt, B. Newnam, R. F. Fisher, and A. B. Swartzlander, “Optical constants for thin films of Ti, Zr, Nb, Mo, Ru, Rh, Pd, Ag, Hf, Ta, W, Re, Ir, Os, Pt, and Au from 24 Å to 1216 Å,” *Appl. Opt.* **27**, 246–278 (1988).  
<sup>18</sup>W. S. Werner, K. Glantschnig, and C. Ambrosch-Draxl, “Optical constants and inelastic electron-scattering data for 17 elemental metals,” *J. Phys. Chem. Ref. Data* **38**, 1013–1092 (2009).  
<sup>19</sup>G. G. Stoney, “The tension of metallic films deposited by electrolysis,” *Proc. R. Soc. London A* **82**, 172–175 (1909).  
<sup>20</sup>J. H. Underwood and E. M. Gullikson, “High-resolution, high-flux, user friendly VLS beamline at the ALS for the 50–1300 eV energy region,” *J. Electr. Spectr. Rel. Phenom.* **92**, 265–272 (1998).  
<sup>21</sup>E. M. Gullikson, S. Mrowka, and B. B. Kaufmann, *Proc. SPIE* **4343**, 363–373 (2001).  
<sup>22</sup>C. P. Jensen, K. K. Madsen, and F. E. Christensen, “Investigation of new material combinations for hard x-ray telescope designs,” *Proc. SPIE* **6266**, 626612 (2006).  
<sup>23</sup>E. M. Gullikson, P. Denham, S. Mrowka, and J. H. Underwood, “Absolute photoabsorption measurements of Mg, Al, and Si in the soft-x-ray region below the L<sub>2,3</sub> edges,” *Phys. Rev. B* **49**, 16283–16288 (1994).  
<sup>24</sup>R. Soufli and E. M. Gullikson, “Optical constants of materials for multilayer mirror applications in the EUV/soft x-ray region,” *Proc. SPIE* **3113**, 222–229 (1997).  
<sup>25</sup>R. Soufli and E. M. Gullikson, “Absolute photoabsorption measurements of molybdenum in the range 60 to 930 eV for optical constant determination,” *Appl. Opt.* **37**, 1713–1719 (1998).  
<sup>26</sup>R. Soufli, A. L. Aquila, F. Salmassi, M. Fernández-Perea, and E. M. Gullikson, “Optical constants of magnetron-sputtered boron carbide thin films from photoabsorption data in the range 30 to 770 eV,” *Appl. Opt.* **47**, 4633–4639 (2008).  
<sup>27</sup>D. L. Windt, “IMD—software for modeling the optical properties of multilayer films,” *Comput. Phys.* **12**, 360–370 (1998).

- <sup>28</sup>R. Soufli and E. M. Gullikson, "Reflectance measurements on clean surfaces for the determination of optical constants of silicon in the extreme ultraviolet-soft-x-ray region," *Appl. Opt.* **36**, 5499–5507 (1997).
- <sup>29</sup>W. R. Hunter, "Measurement of optical properties of materials in the vacuum ultraviolet spectral region," *Appl. Opt.* **21**, 2103–2114 (1982).
- <sup>30</sup>M. Altarelli, D. L. Dexter, H. M. Nussenzweig, and D. Y. Smith, "Superconvergence and sum rules for the optical constants," *Phys. Rev. B* **6**, 4502–4509 (1972).
- <sup>31</sup>A. D. Rakić, A. B. Djurišić, J. M. Elazar, and M. L. Majewski, "Optical properties of metallic films for vertical-cavity optoelectronic devices," *Appl. Opt.* **37**, 5271–5283 (1998).
- <sup>32</sup>C. T. Chantler, "Theoretical form factor, attenuation and scattering tabulation for  $Z = 1-92$  from  $E = 1-10$  eV to  $E = 0.4-1.0$  MeV," *J. Phys. Chem. Ref. Data* **24**, 71–643 (1995); see <http://physics.nist.gov/ffast> for an updated version of X-ray Form Factor, Attenuation and Scattering Tables (Version 2.1) (National Institute of Standards and Technology, Gaithersburg, MD, 2005).
- <sup>33</sup>F. Delmotte, J. Meyer-Ilse, F. Salmassi, R. Soufli, C. Burcklen, J. Rebelatto, A. Jérôme, I. Vickridge, E. Briand, and E. Gullikson, "Soft x-ray optical constants of sputtered chromium thin films with improved accuracy in the L and M absorption edge regions," *J. Appl. Phys.* **124**, 035107 (2018).
- <sup>34</sup>D. Y. Smith and E. Shiles, "Finite-energy f-sum rules for valence electrons," *Phys. Rev. B* **17**, 4689–4694 (1978).
- <sup>35</sup>L. V. Rodríguez-de Marcos, J. A. Méndez, and J. I. Larruquert, "Tuning sum rules with window functions for optical constant evaluation," *J. Opt.* **18**, 075606 (2016).